Organometallic Halides

Deutsche Ausgabe: DOI: 10.1002/ange.201601933
Internationale Ausgabe: DOI: 10.1002/anie.201601933

A Photoferroelectric Perovskite-Type Organometallic Halide with Exceptional Anisotropy of Bulk Photovoltaic Effects

*Zhihua Sun, Xitao Liu, Tariq Khan, Chengmin Ji, Muhammad Adnan Asghar, Sangen Zhao, Lina Li, Maochun Hong, and Junhua Luo**

Abstract: *Perovskite-type ferroelectrics composed of organometallic halides are emerging as a promising alternative to conventional photovoltaic devices because of their unique photovoltaic effects (PVEs). A new layered perovskite-type photoferroelectric, bis(cyclohexylaminium) tetrabromo lead (**1**), is presented. The material exhibits an exceptional anisotropy of bulk PVEs. Upon photoexcitation, superior photovoltaic behaviors are created along its inorganic layers, which are composed of corner-sharing $PbBr_6$ octahedra. Semiconducting activity with remarkable photoconductivity is achieved in the vertical direction, showing sizeable on/off current ratios ($>10^4$), which compete with the most active photovoltaic material $CH_3NH_3PbI_3$. In **1** the temperature-dependence of photovoltage coincides fairly well with that of polarization, confirming the dominant role of ferroelectricity in such highly anisotropic PVEs. This finding sheds light on bulk PVEs in ferroelectric materials, and promotes their application in optoelectronic devices.*

Bulk photovoltaic effects (PVEs) of the photosensitive ferroelectrics (termed photoferroelectrics) are appealing optoelectronic elements because of their unique features, which include, large photovoltages, high carrier mobility, and steady-state photocurrent in a homogeneous medium.[1,2] Hence, high-performance photoferroelectrics are a promising alternative to conventional photovoltaic materials, including those that are used in electroluminescent devices and solar cells.[3,4] Ultrahigh open-circuit photovoltages can be generated in photoferroelectrics, which breaks through the band gap limitation of conventional *p-n* and heterojunction-type photovoltaic devices. For instance, an anomalously high photovoltage of approximately 16 V was achieved with $BiFeO_3$ crystallites, far exceeding the intrinsic band gap value of the material ($E_g \approx 2.67$ eV).[5] Improvements in power conversion efficiency are expected upon introduction of ferroelectric PVEs because of the built-in electric field induced by spontaneous polarization.[3a,4] This fascinating effect suggests that ferroelectric materials are viable photovoltaic candidates capable of harvesting energy from light.[6] However, studies to date have focused on ferroelectric PVEs derived from inorganic oxides, such as $LiNbO_3$,[7] $Pb(ZrTi)O_3$,[8] and $BiFeO_3$.[9] Although ferroelectric PVEs have stimulated intensive research in the last decade, it remains challenging to design photoferroelectric candidates because of a lack of knowledge regarding the conclusive mechanism and origin of ferroelectric PVEs.[6] Perovskite-type organometallic hybrids, which benefit from the structural flexibility and tunability of assemblies constructed from both inorganic and organic building blocks, are promising photoferroelectrics.[1] In these compounds, inorganic MX_6 octahedra frame a channel that allows substantial freedom of movement of organic components; this attribute favors ferroelectricity.[10] Moreover, their electronic structures and electrical properties (such as band gap and charge carrier transport), can be feasibly modulated by chemical modification. For example, a recent report shows that the band gap values of $CH_3NH_3PbX_3$ (X = Cl, Br, I) can be controlled by chemical substitution.[11] In this way an impressive photocurrent (ca. 20 mA cm^{-2}) was obtained with a $CH_3NH_3PbI_3$ photovoltaic device.[11b] Nevertheless, in the case of $CH_3NH_3PbI_3$, ferroelectric activity and the micro-origin of photo-excited behaviors is still largely unknown.[12] In this context, development of new photoferroelectrics is crucial to improve our collective understanding of ferroelectric PVEs and to ascertain the applicability of these materials in photovoltaics.

Herein, we report a layered perovskite-type photoferroelectric material, bis(cyclohexylaminium) tetrabromo lead (**1**), which exhibits promising bulk PVEs along with exceptional anisotropy. Significant photoconductivity is observed in the vertical direction (with respect to the material's polar axis), with a sizeable on/off current ratio greater than 10^4. Superior photovoltaic activity occurs along the inorganic layers of the corner-sharing $PbBr_6$ octahedra. To the best of our knowledge, **1** is the first example of a perovskite-type hybrid ferroelectric, showing temperature-dependent photovoltage, and thereby confirming that ferroelectric polarization dominates bulk PVEs. Such findings provide a critical insight into ferroelectric PVEs, and promote their application in optoelectronic devices.

Single-crystals of **1** were generated from saturated solutions of precursor materials (elongation is observed along the crystallographic *c*-axis; Supporting Information, Figures S1 and S2), and purity was confirmed by powder X-ray diffraction (Supporting Information, Figure S3). Compound **1**

[*] Dr. Z. Sun, C. Ji, Dr. S. Zhao, Dr. L. Li, Prof. M. Hong, Prof. J. Luo
State Key Laboratory of Structural Chemistry, Fujian Institute of Research on the Structure of Matter, Chinese Academy of Sciences
Fuzhou, Fujian, 350002 (P.R. China)
Dr. Z. Sun, Dr. X. Liu, T. Khan, C. Ji, M. A. Asghar, Dr. S. Zhao, Dr. L. Li, Prof. M. Hong, Prof. J. Luo
Key Laboratory of Optoelectronic Materials Chemistry and Physics, Fujian Institute of Research on the Structure of Matter, Chinese Academy of Sciences
Fuzhou, Fujian, 350002 (P.R. China)
E-mail: jhluo@fjirsm.ac.cn

Supporting information for this article can be found under: http://dx.doi.org/10.1002/anie.201601933.

crystallizes in the orthorhombic system with a polar space group of $Cmc2_1$ at room temperature.[13] The solid state structure of **1** features a typical organic–inorganic layered perovskite-type architecture with the general formula A_2BX_4 (A = monovalent organic ammonium, B = divalent transition metal, X = halogen), containing infinite, staggered layers of corner-sharing MX_6 octahedra interleaved by organic ammonium cations.[14] This is slightly different from that of the cubic ABX_3 perovskites, in which the organic cation is at the center of the cavity formed by the B and X ions. The $PbBr_6$ group adopts a distorted octahedral configuration, as indicated by the Pb–Br bond lengths (Figure 1a). Corner-sharing $PbBr_6$

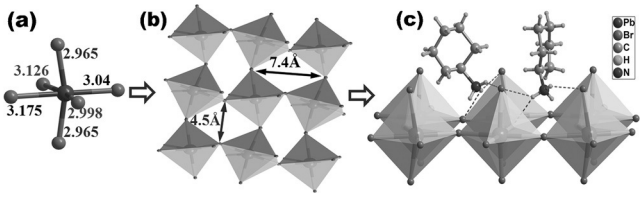

Figure 1. a) The $PbBr_6$ octahedron. b) Inorganic layer of the corner-sharing $PbBr_6$ octahedra. Differing diagonal distances reveal a distorted square. c) Organic cations are bound to inorganic octahedra through N–H···Br hydrogen bonds, as shown by dashed lines.

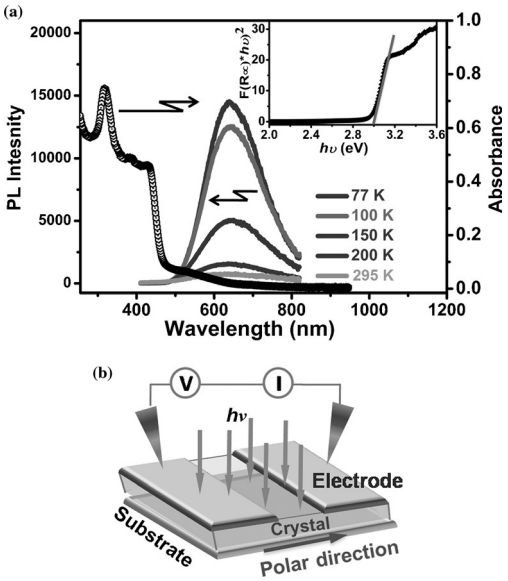

Figure 2. a) Optical absorption and PL spectra for **1**. Inset: the band gap obtained from optical spectra. b) Schematic diagram of an electrical lateral architecture for investigating bulk PVEs. Symmetric top electrodes with an inter-electrode distance of ca. 0.3 mm were fabricated on the crystal surface.

octahedra are bridged by bromide in infinite inorganic layers, which lie on the crystallographic *bc*-plane (Supporting Information, Figure S4). The inorganic sheets imbue **1** with semiconducting properties and appreciable carrier transport behavior (that is, high carrier mobility and long diffusion length), which are important from a photovoltaic point of view. Four neighboring lead atoms and the adjacent Pb-Br-Pb bonding-edges create a distorted square, as revealed by a comparison of diagonal lengths (Figure 1b). Ammonium counter-cations are situated inside cavities and are bonded to the $PbBr_6$ octahedra through N–H···Br hydrogen bonds (Figure 1c; Supporting Information, Figure S6), while the cyclohexane rings orient outside the cavity. This alignment allows reorientation of cyclohexane rings, which consequently appear disordered in the crystal structure determination. Accordingly, the inorganic layers of corner-sharing $PbBr_6$ octahedra are interleaved by the bilayers of organic ammonium cations, creating an architecture analogous with perovskite-type hybrids, such as $(cyclopentylaminium)_2PbI_4$,[15a] $(heptylaminium)_2PbI_4$,[15b] and $(benzylaminium)_2PbCl_4$.[15c]

Generally, band gap magnitude is critical for absorbing photon energies through PVEs;[16] a small band gap is required for photovoltaic materials. The optical diffuse reflectance of **1** shows an absorption edge at about 420 nm (Figure 2a), which is comparable with other perovskite hybrids of $(R\text{-}NH_3)_2PbCl_4$,[17] but smaller than that for $CH_3NH_3PbI_3$.[18] Using a Tauc plot, the band gap for **1** was estimated to be approximately 2.95 eV (intercept value of a plot of $(F(R_\infty)h\nu)^{1/m}$ vs. light energy; inset in Figure 2a). This value agrees well with the ab initio calculation of the band structure (ca. 2.95 eV; Supporting information), and is lower than that of some inorganic oxides, such as $LiNbO_3$, $BaTiO_3$, and $Pb(ZrTi)O_3$ (larger than 3.0 eV).[9a] Moreover, the photoluminescence (PL) spectrum exhibits an extensive emission peak at about 562 nm ($\lambda_{ex} = 420$ nm), which is distinctly red-shifted in comparison with the absorption onset. This implies that the excited PL light can be easily distinguished from the absorbed light, which would be advantageous in photovoltaic applications.[19]

Bulk PVEs of **1** were investigated using a lateral device architecture (Figure 2b), and photo-excitation was performed under a light source with a photon energy of 2.95 eV (Xenon lamp).[9a] The black circles in Figure 3a represent the "dark current" without illumination, while purple and orange traces show the current–voltage (*I–V*) characteristics under different light intensities. The dark *I–V* traces fit well with the Mott–Gurney law of power dependence, demonstrating an ohmic region at lower bias and a space charge limited current model at higher bias. The trap density (n_{traps}) was estimated to be approximately 1.1×10^{10} cm^{-3}, smaller than that of $CH_3NH_3PbI_3$ crystals.[19] When compared to established inorganic semiconductors, including silicon ($n_{traps} = 10^{13}$–10^{14} cm^{-3}) and CdTe ($n_{traps} = 10^{11}$–10^{13} cm^{-3}),[20] Figure 3a reveals the high crystalline quality of **1**. Upon photo-excitation, enhanced currents were coupled with increased conductivity (Figure 3a). Photocurrent increased by three orders of magnitude, changing from 0.85 pA (dark) to 4.1 nA (at 80 mW cm^{-2}). The on/off ratio of current was estimated to be about 10^4, which is almost on par with that of $(CH_3NH_3)PbI_3$,[11b] and much larger than that observed in thin films or bad insulator crystals.[21] This feature indicates that **1** has potential as a photodetector.[22] Moreover, variable photoconductivity at different illumination intensities reveals that the semiconducting properties of **1** coincide well with its temperature-dependent conductivity (Supporting Information, Figure S7). Promisingly, bulk PVEs are clearly observed

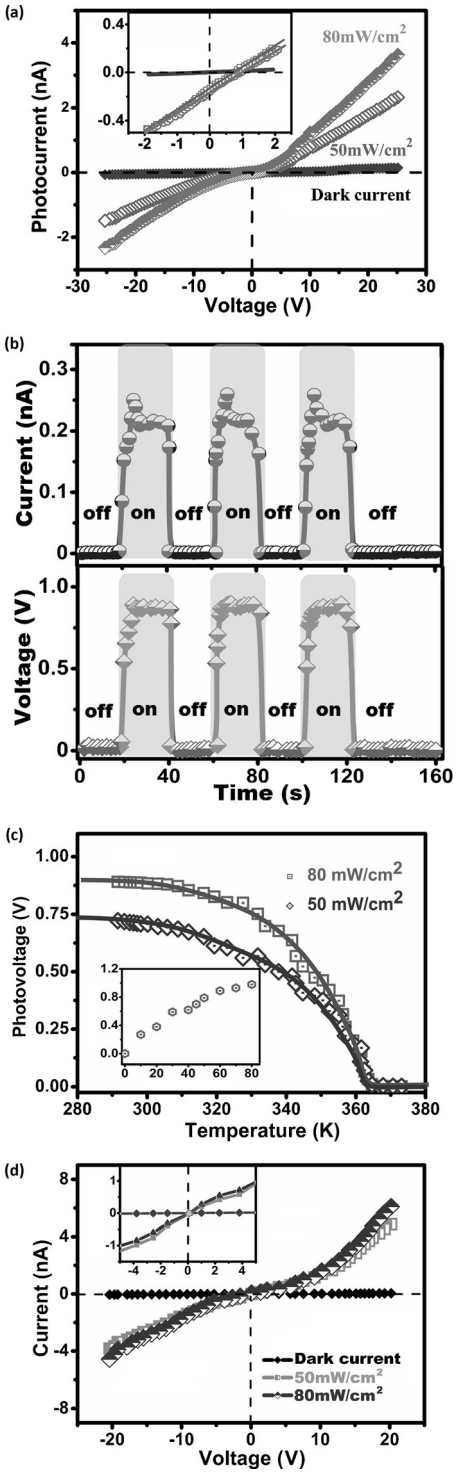

Figure 3. a) Bulk PVEs of **1** measured under different light intensities. Inset: expansion around the zero field. b) Repeated bulk PVEs of photocurrent and photovoltage, achieved by periodic switching of a light source. c) Temperature-dependence of photovoltage. Inset: y-axis (Voltage (V)) vs. x-axis (Power (mW/cm^2)). d) Significant photoconductivity in the direction vertical with respect to the *c*-axis. Inset: expanded view of *I–V* curves near the zero field.

from the *I–V* traces, including the open circuit voltage (V_{oc}) of $+0.98$ V and short circuit current (I_{sc}) of -0.25 nA ($J_{sc} \approx 55\ nA\,cm^{-2}$; inset in Figure 3a). Although such characteristics are inferior to tip-enhanced ferroelectric PVEs at domain boundaries,[23] they are comparable with other photovoltaic devices based on $BiFeO_3$ crystals[21] and lead lanthanum zirconate titanate (PLZT) ceramics.[24] The relatively low V_{oc} and I_{sc} may be attributed to charge-trapping by interfacial effects at metal–crystal interfaces.[25] Notably, the time-resolved repeatable switching of PVEs in **1** (achieved by turning light on/off) shows little temporal change in photocurrent and photovoltage (stability is shown after ca. 10^3 cycles; Figure 3b). Such high stability over multiple cycles is advantageous for photovoltaic applications.[26]

Bulk PVEs of **1** exhibits an unambiguous photovoltage temperature-dependence (Figure 3c). Photovoltage shows a gradual decline as temperature increases, and disappears completely above the Curie temperature point ($T_c = 364$ K), which coincides well with that of spontaneous polarization (as discussed below). Moreover, V_{oc} is dependent on light intensity and exhibits a linear trend (Figure 3c inset), which suggests that higher photovoltages could be expected under higher incident power. To the best of our knowledge, this is the first example of temperature-dependent PVEs observed in organometallic hybrid ferroelectrics; the finding is presented in conjunction with ferroelectric polarization. Related studies have been reported on *p-n* junction or heterojunction-type devices.[27] Another striking feature, is the unpredictable anisotropy of PVEs in **1**; distinct photoelectric behaviors are excited along different directions. As described above, superior PVEs are generated parallel to the polar-axis of the material, including superior photovoltage and large in-plane photocurrent. In contrast, significant photoconductivity is recorded in a vertical direction with respect to the *c*-axis of the crystallographic unit cell (Figure 3d), showing almost negligible levels of PVEs (Figure 3d inset). Contrary to the behavior observed in typical semiconductor *p-n* junctions, this suggests that the depolarization electric field in **1** affords a driving force for photocurrent. Since the origin of ferroelectric PVEs is complicated, several mechanisms have been proposed, such as depolarization electric field effects, optical rectification effects, and asymmetry potentials.[28] All mechanisms state that polarization makes an important contribution to ferroelectric PVEs. The exceptional anisotropy and temperature-dependent photovoltage properties of **1** suggest that bulk PVEs are strongly involved with the internal electric field stemming from intrinsic spontaneous polarization.

To reveal the relationship between ferroelectricity and PVEs, we studied the ferroelectric properties of **1**. Differential scanning calorimetry (DSC) and temperature-dependent second harmonic generation (SHG) effects reveal that **1** undergoes a phase transition at 364 K (Supporting Information, Figures S7–10). A remarkable change in SHG signals at T_c indicates a structural transition from a centrosymmetric state ($T > T_c$) to an acentric phase ($T < T_c$),[29,30] with an SHG susceptibility of about $1.2\ pm\,V^{-1}$ ($3.0 \times$ KDP (potassium dihydrogen phosphate)). This value reveals disruption to symmetry in **1**, which is one of the defining characteristics of ferroelectrics.[31] Dielectric constants measured along the polar *c*-axis display large anomalies at T_c, ranging from less than 50 to 420 (Supporting Information, Figure S10), and are reminiscent of ferroelectric activities. Most importantly, the

switchable polarization of **1** is revealed by *P*–*E* hysteresis loops. At 369 K, the linear curve of *P*--*E* dependence reveals a paraelectric property. Below T_c, ferroelectric loops typical of nonlinear dielectric responses were recorded, affording a value of 6.6 $\mu C cm^{-2}$ and remanent polarization of 6.5 $\mu C cm^{-2}$ (Figure 4a). Polarization was also investigated by assessment of pyroelectric effects. A sharp current peak was created to compensate charge displacement at T_c (Figure 4b), affording the P_s value of 6.8 $\mu C cm^{-2}$, which agrees with the measured hysteresis loops. All results (DSC, SHG, and electric measurements) indicate that **1** is a ferroelectric material, and that its bulk PVEs are strongly associated with ferroelectric activities.

Directional structures of **1** were analyzed to probe the microscopic origin of the highly anisotropic PVEs. For the ferroelectric phase (FEP), an asymmetric configuration of the apical Pb–Br bonds (2.965 Å) and bridging bonds (2.998, 3.04, 3.126, and 3.175 Å) reveals a high degree of distortion in $PbBr_6$ octahedra (Figure 1a). Notably, all distorted $PbBr_6$ octahedra exhibit a coherent displacement, with Br-Pb-Br bond angles deviating from 90° within the crystallographic *bc* plane (Supporting Information, Figure S4). Thus, the negatively charged centers of $PbBr_6$ octahedra apparently move in the direction of the c^--axis. Meanwhile, the bilateral organic moieties capping the inorganic sheets also display a coherent performance, and tilt in the opposite direction along the c^+-axis, which is also implied by the corresponding N–H···Br hydrogen bonds (Figure 5a). The coupling of these characteristics leads to separation of positive and negative charge centers, prompting formation of dipole moments (4.9×10^{-29} C m; Supporting information) and ferroelectric polarization along the *c*-axis (Figure 5b). In contrast, all the molecular dipoles show equivalent motional components along *a*- and *b*-axes, eliminating the possibility of electric polarization. For instance, each $PbBr_6$ octahedron shifts towards the neighboring moiety in an opposite manner, thereby counteracting the occurrence of dipolar components (Figure 5c). Similarly, equivalence is established for the organic counterparts (white arrows in Figure 5c), which leads to a counteractive dipole-reorientation and removal of polarization.[32]

Additionally, the origin of temperature-dependent PVEs in **1** was elucidated by analyzing variable-temperature crystal structures. For the paraelectric phase (PEP), the most striking feature of **1** is symmetry restoration from a polar ($Cmc2_1$) to nonpolar (*Cmca*) lattice.[13] The geometric constraints of the inorganic sheets cause the $PbBr_6$ octahedra to adopt a highly symmetric configuration (Figure 5a). Such a transformation results from the titling or rotational motions of $PbBr_6$ octahedra inside inorganic sheets (Supporting Information, Figure S5), a characteristic resembling Jahn–Teller distortion of the CuX_6 octahedra in Cu^{II}-based compounds.[33] Furthermore, organic counterparts reveal a disordered atomic arrangement, which satisfies the requirements of crystallographic symmetry. As expected, all components adopt a highly symmetric prototypic geometry, which excludes molecular dipole moments and polarization (Figure 5d). It is difficult to create a built-in electric field using ferroelectric polarization, and thus, **1** presents a negligible photovoltage above T_c.

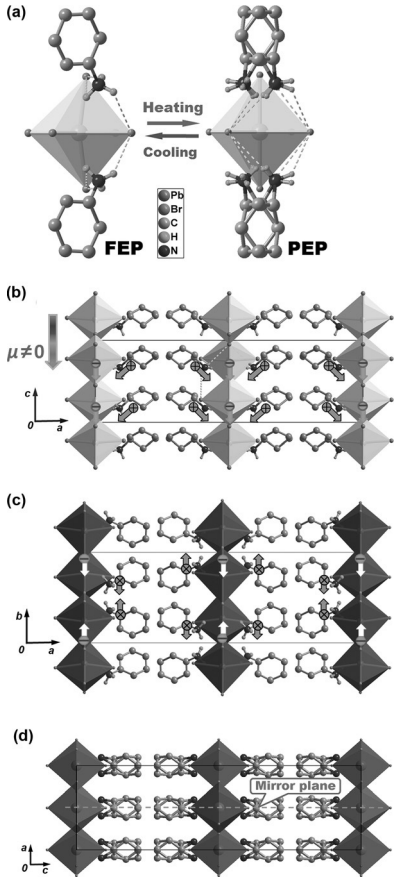

Figure 5. a) Molecular structures of **1** at FEP and PEP. b) Packing diagram viewed along the *b*-axis and c) *c*-axis at FEP. Arrows indicate the dipole moments ($\mu \neq 0$) induced by separation of positive and negative charges. d) The packing structure of **1** viewed along the *b*-axis at PEP. Dashed lines depict the N–H···Br hydrogen bonds. Hydrogen atoms bonded to carbon atoms are omitted for clarity.

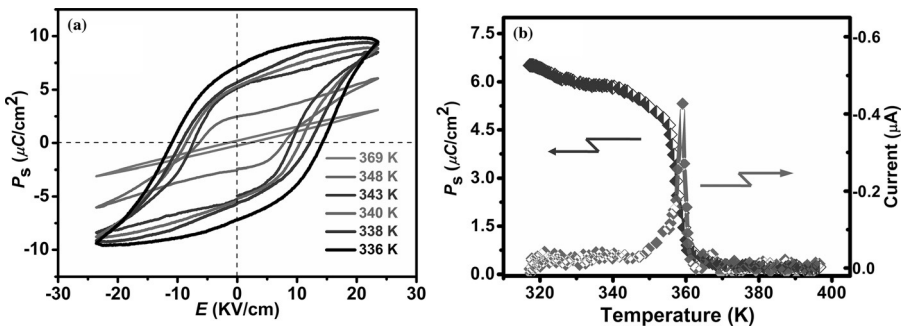

Figure 4. Ferroelectric properties of **1**. a) Spontaneous polarization and electric field (*P*–*E*) loops measured along the *c*-axis at different temperatures. b) Pyroelectric current measurement. The temperature-dependence of spontaneous polarization was obtained by integrating the pyroelectric currents.

In summary, we have successfully reported a layered perovskite-type photoferroelectric, which exhibits promising bulk PVEs along with an exceptional anisotropy. The appreciable photoconductivity of **1** is comparable with that of $CH_3NH_3PbI_3$. In particular, the temperature-dependent photovoltage of **1** coincides well with polarization characteristics, revealing that PVEs are likely to be involved with ferroelectricity. Structural analysis afforded a comprehensive understanding of the relationship between PVEs and ferroelectricity. Since perovskite-type hybrid ferroelectrics benefit from structural variability and tunability, fine-tuning of inorganic and/or organic components should allow optimization of their electronic and optical properties. This work enriches the understanding of PVEs in ferroelectrics, and presents opportunities for innovative application of ferroelectrics in photodevices, such as photoelectrochemical cells and photosensitive sensors.

Acknowledgements

This work was supported by NSFC (21525104, 91422301, 21373220, 51402296, 21571178, 51502288, 51502290, and 21301172), the NSF for Distinguished Young Scholars of Fujian Province (2014J06015), NSF of Fujian Province (2014J01067, 2014J05068 and 2015J05040), Youth Innovation Promotion of CAS (2014262, 2015240, 2016274), and "Chunmiao Projects" of Haixi Institute of Chinese Academy of Sciences (CMZX-2013-002 and CMZX-2015-003).

Keywords: ferroelectric materials · organometallic halides · perovskite · photovoltaic effects

How to cite: *Angew. Chem. Int. Ed.* **2016**, *55*, 6545 – 6550
Angew. Chem. **2016**, *128*, 6655 – 6660

[1] a) V. M. Fridkin, *Photoferroelectrics*, Springer, Heidelberg, **1979**; b) B. I. Sturman, V. M. Fridkin, *The Photovoltaic and Photorefractive Effects in Noncentrosymmetric Materials*, Gordon and Breach, Newark, **1992**.

[2] V. K. Wadhawan, *Introduction to Ferroic Materials*, Gordon and Breach, Newark, **2000**.

[3] a) T. Choi, S. Lee, Y. J. Choi, V. Kiryukhin, S.-W. Cheong, *Science* **2009**, *324*, 63 – 66; b) B. Kundys, M. Viret, D. Colson, D. O. Kundys, *Nat. Mater.* **2010**, *9*, 803 – 805; c) R. Nechache, C. Harnagea, S. Li, L. Cardenas, W. Huang, J. Chakrabartty, F. Rosei, *Nat. Photonics* **2015**, *9*, 61 – 67.

[4] a) J. Kreisel, M. Alexe, P. A. Thomas, *Nat. Mater.* **2012**, *11*, 260; b) F. Wang, S. Young, F. Zheng, I. Grinberg, A. M. Rappe, *Nat. Commun.* **2016**, *7*, 10419.

[5] S. Y. Yang, J. Seidel, S. J. Byrnes, P. Shafer, C.-H. Yang, M. D. Rossell, P. Yu, Y.-H. Chu, J. F. Scott, J. W. Ager III, L. W. Martin, R. Ramesh, *Nat. Nanotechnol.* **2010**, *5*, 143 – 147.

[6] H. Huang, *Nat. Photonics* **2010**, *4*, 134 – 135.

[7] a) L. Arizmendi, *Phys. Status Solidi A* **2004**, *201*, 253 – 258; b) B. Kang, B. K. Rhee, G.-T. Joo, S. Lee, K.-S. Lim, *Opt. Commun.* **2006**, *266*, 203 – 206.

[8] a) M. Ichiki, Y. Morikawa, T. Nakada, *Jpn. J. Appl. Phys.* **2002**, *41*, 6993 – 6996; b) F. Zheng, J. Xu, L. Fang, M. Shen, X. Wu, *Appl. Phys. Lett.* **2008**, *93*, 172101; c) M. Qin, K. Yao, Y. C. Liang, *Appl. Phys. Lett.* **2008**, *93*, 122904.

[9] a) Y. Yuan, Z. Xiao, B. Yang, J. Huang, *J. Mater. Chem. A* **2014**, *2*, 6027 – 6041; b) W. Ji, K. Yao, Y. C. Liang, *Adv. Mater.* **2010**, *22*, 1763 – 1766; c) D. Cao, Z. Wang, Nasori, L. Wen, Y. Mi, Y. Lei, Angew. Chem. Int. Ed. **2014**, *53, 11027 – 11031; Angew. Chem.* **2014**, *126*, 11207 – 11211; *Angew. Chem.* **2014**, *126*, 11207 – 11211.

[10] a) D.-W. Fu, W. Zhang, H.-L. Cai, Y. Zhang, J.-Z. Ge, R.-G. Xiong, S. D. Huang, T. Nakamura, *Angew. Chem. Int. Ed.* **2011**, *50*, 11947 – 11951; *Angew. Chem.* **2011**, *123*, 12153 – 12157; b) G.-C. Xu, W. Zhang, X.-M. Ma, Y.-H. Chen, L. Zhang, H.-L. Cai, Z.-M. Wang, R.-G. Xiong, S. Gao, *J. Am. Chem. Soc.* **2011**, *133*, 14948 – 14951; c) H.-Y. Ye, Y. Zhang, D.-W. Fu, R.-G. Xiong, *Angew. Chem. Int. Ed.* **2014**, *53*, 11242 – 11247; *Angew. Chem.* **2014**, *126*, 11424 – 11429.

[11] a) E. Mosconi, A. Amat, M. K. Nazeeruddin, M. Grätzel, F. De Angelis, *J. Phys. Chem. C* **2013**, *117*, 13902 – 13913; b) Z. Xiao, Y. Yuan, Y. Shao, Q. Wang, Q. Dong, C. Bi, P. Sharma, A. Gruverman, J. Huang, *Nat. Mater.* **2015**, *11*, 193 – 198.

[12] a) Y. Kutes, L. Ye, Y. Zhou, S. Pang, B. D. Huey, N. P. Padture, *J. Phys. Chem. Lett.* **2014**, *5*, 3335 – 3339; b) J. M. Frost, K. T. Butler, F. Brivio, C. H. Hendon, M. van Schilfgaarde, A. Walsh, *Nano Lett.* **2014**, *14*, 2584 – 2590; c) H.-S. Kim, S. K. Kim, B. J. Kim, K.-S. Shin, M. K. Gupta, H. S. Jung, S.-W. Kim, N.-G. Park, *J. Phys. Chem. Lett.* **2015**, *6*, 1729 – 1735; d) A. Pecchia, D. Gentilini, D. Rossi, M. A. der Maur, A. D. Carlo, *Nano Lett.* **2016**, *16*, 988 – 992.

[13] Crystal data for **1:** $T = 170$ K, $M_r = 727.19$, Orthorhombic, $Cmc2_1$, $a = 27.7379(12)$, $b = 8.6547(3)$, $c = 8.2240(4)$ Å, $V = 1974.28(15)$ Å^3, $Z = 4$, $\rho_{cal.} = 2.447$ g cm^{-3}, $S = 1.079$, $R_1(I > 2\sigma(I)) = 0.0307$, $wR_2(I > 2\sigma(I)) = 0.0744$; $T = 373$ K, $C_{12}H_{28}Br_4N_2Pb$, $M_r = 727.19$, Orthorhombic, $Cmca$, $a = 28.5200(10)$, $b = 8.5376(2)$, $c = 8.4503(2)$ Å, $V = 2057.58(10)$ Å^3, $Z = 4$, $\rho_{cal.} = 2.444$ g cm^{-3}, $S = 1.623$, $R_1(I > 2\sigma(I)) = 0.0784$, wR_2 $(I > 2\sigma(I)) = 0.2111$.

[14] a) D. G. Billing, A. Lemmerer, *CrystEngComm* **2009**, *11*, 1549 – 1562; b) H.-Y. Ye, W.-Q. Liao, C.-L. Hu, Y. Zhang, Y.-M. You, J.-G. Mao, P.-F. Li, R.-G. Xiong, *Adv. Mater.* **2016**, *28*, 2579 – 2586.

[15] a) D. G. Billing, A. Lemmerer, *CrystEngComm* **2007**, *9*, 236 – 244; b) A. Lemmerer, D. G. Billing, *Dalton Trans.* **2012**, *41*, 1146 – 1157; c) W.-Q. Liao, Y. Zhang, C.-L. Hu, J.-G. Mao, H.-Y. Ye, P.-F. Li, S. D. Huang, R.-G. Xiong, *Nat. Commun.* **2015**, *6*, 7388.

[16] I. Grinberg, D. V. West, M. Torres, G. Gou, D. M. Stein, L. Wu, G. Chen, E. M. Gallo, A. R. Akbashev, P. K. Davies, J. E. Spanier, A. M. Rappe, *Nature* **2013**, *503*, 509 – 512.

[17] S. Zhang, P. Audebert, Y. Wei, J.-S. Lauret, L. Galmiche, E. Deleporte, *J. Mater. Chem.* **2011**, *21*, 466 – 474.

[18] L. Dimesso, M. Dimamay, M. Hamburger, W. Jaegermann, *Chem. Mater.* **2014**, *26*, 6762 – 6770.

[19] Y. Liu, Z. Yang, D. Cui, X. Ren, J. Sun, X. Liu, J. Zhang, Q. Wei, H. Fan, F. Yu, X. Zhang, C. Zhao, S. Liu, *Adv. Mater.* **2015**, *27*, 5176 – 5183.

[20] a) J. R. Ayres, *J. Appl. Phys.* **1962**, *33*, 1733 – 1737; b) I. Capan, V. Borjanović, B. Piva, *Sol. Energy Mater. Sol. Cells* **2007**, *91*, 931 – 937; c) A. Balcioglu, R. K. Ahrenkiel, F. Hasoon, *J. Appl. Phys.* **2000**, *88*, 7175 – 7178.

[21] R. Moubah, O. Rousseau, D. Colson, A. Artemenko, M. Maglione, M. Viret, *Adv. Funct. Mater.* **2012**, *22*, 4814 – 4818.

[22] M. C. Tarun, F. A. Selim, M. D. McCluskey, *Phys. Rev. Lett.* **2013**, *111*, 187403.

[23] M. Alexe, D. Hesse, *Nat. Commun.* **2011**, *2*, 256.

[24] M. Ichiki, R. Maeda, Y. Morikawa, Y. Mabune, T. Nakada, K. Nonaka, *Appl. Phys. Lett.* **2004**, *84*, 395 – 397.

[25] S. Habicht, R. J. Nemanich, A. Gruverman, *Nanotechnology* **2008**, *19*, 495303.

[26] S. R. Wenham, M. A. Green, M. E. Watt, R. Corkish, *Applied Photovoltaics*, Earthscan, Ltd. **2006**.

[27] J. R. Sun, B. G. Shen, Z. G. Sheng, Y. P. Sun, *Appl. Phys. Lett.* **2004**, *85*, 3375 – 3377.
[28] a) M. Bass, P. A. Franken, J. F. Ward, G. Weinreich, *Phys. Rev. Lett.* **1962**, *9*, 446 – 448; b) J. Junquera, P. Ghosez, *Nature* **2003**, *422*, 506 – 509; c) H. T. Yi, T. Choi, S. G. Choi, Y. S. Oh, S.-W. Cheong, *Adv. Mater.* **2011**, *23*, 3403 – 3407.
[29] H.-L. Cai, W. Zhang, J.-G. Ge, Y. Zhang, K. Awaga, T. Nakamura, R.-G. Xiong, *Phys. Rev. Lett.* **2011**, *107*, 147601.
[30] Z. Sun, J. Luo, C. Ji, S. Zhang, S.-H. Li, F. Deng, M. Hong, *Adv. Mater.* **2013**, *25*, 4159 – 4163.
[31] a) W. Zhang, R.-G. Xiong, *Chem. Rev.* **2012**, *112*, 1163 – 1195; b) D.-W. Fu, H.-L. Cai, Y. Liu, Q. Ye, W. Zhang, Y. Zhang, X.-Y. Chen, G. Giovannetti, M. Capone, J. Li, R.-G. Xiong, *Science* **2013**, *339*, 425 – 428.
[32] M. E. Lines, A. M. Glass, *Principles and Applications of Ferroelectrics and Related Materials*, Oxford University Press, New York, **2001**.
[33] D. B. Mitzi, C. D. Dimitrakopoulos, L. L. Kosbar, *Chem. Mater.* **2001**, *13*, 3728 – 3740.

Received: February 24, 2016
Revised: March 20, 2016
Published online: April 18, 2016

